

# Agricultural runoff fuels large phytoplankton blooms in vulnerable areas of the ocean

J. Michael Beman<sup>1</sup>, Kevin R. Arrigo<sup>2</sup> & Pamela A. Matson<sup>1,3</sup>

<sup>1</sup>Department of Geological and Environmental Sciences, <sup>2</sup>Department of Geophysics and <sup>3</sup>School of Earth Sciences, Stanford University, Stanford, California 94305, USA

Biological productivity in most of the world's oceans is controlled by the supply of nutrients to surface waters. The relative balance between supply and removal of nutrients—including nitrogen, iron and phosphorus—determines which nutrient limits phytoplankton growth. Although nitrogen limits productivity in much of the ocean<sup>1,2</sup>, large portions of the tropics and subtropics are defined by extreme nitrogen depletion. In these regions, microbial denitrification removes biologically available forms of nitrogen from the water column, producing substantial deficits relative to other nutrients<sup>3–5</sup>. Here we demonstrate that nitrogen-deficient areas of the tropical and subtropical oceans are acutely vulnerable to nitrogen pollution. Despite naturally high nutrient concentrations and productivity<sup>6–8</sup>, nitrogen-rich agricultural runoff fuels large (54–577 km<sup>2</sup>) phytoplankton blooms in the Gulf of California. Runoff exerts a strong and consistent influence on biological processes, in 80% of cases stimulating blooms within days of fertilization and irrigation of agricultural fields. We project that by the year 2050, 27–59% of all nitrogen fertilizer will be applied in developing regions located upstream of nitrogen-deficient marine ecosystems. Our findings highlight the present and future vulnerability of these ecosystems to agricultural runoff.

Throughout large areas of the ocean, nitrogen (N) deficits characterize regions of active marine microbial denitrification<sup>3–5</sup>. In these areas, biological productivity generates large amounts of organic material, the decomposition of which depletes water column oxygen concentrations, resulting in a low-oxygen environment that is favourable to denitrification. The Gulf of California (GOC, Fig. 1) contains some of the highest nutrient concentrations in the oceans<sup>7</sup> and sustains highly elevated rates of biological productivity<sup>6</sup>. Supplied by wind-driven upwelling<sup>8</sup> and inflow of nutrient-rich waters at depth<sup>9</sup>, concentrations of nitrogen and phosphorus (P) are well-correlated, and found in proportions corresponding to the Redfield N:P ratio of 16:1 (ref. 7). As phytoplankton growth reduces available N concentrations to near zero, an excess of nearly 1 μM P remains, suggesting a deficit of 16 μM N relative to P (ref. 7).

Although N deficits may increase vulnerability to exogenous sources of N, how the GOC and other N-deficient areas of the ocean respond to anthropogenic nitrogen pollution is largely unknown. In marine ecosystems, N pollution is associated with increased phytoplankton biomass and rates of primary production, the formation of harmful (often toxic) algal blooms, and low-oxygen conditions<sup>10</sup>. Inarguably, the effects of marine N pollution are becoming increasingly widespread and severe as a consequence of the global expansion of industrialized agriculture and the intensification of current practices. N-based agricultural fertilizers are the primary source of N pollution, and their use is predicted to double or triple over the next 50 years<sup>11</sup>.

Fertilizer application rates are extremely high (250 kg N ha<sup>-1</sup>, ref. 12) in the Yaqui Valley, a 2.25 × 10<sup>5</sup> ha agricultural system located along the east coast of the GOC (Fig. 1). Surface water runoff from the Yaqui Valley is determined almost entirely by irrigation of agricultural fields, and results in the loss of large pulses of N to the

atmosphere, ground water and surface waters of the valley during irrigation events<sup>13–16</sup>. Nearly 66% of the N applied in fertilizer is lost from the Yaqui Valley, 20–40% of which is lost in surface waters<sup>14,16</sup>. Irrigation events are synchronized throughout the valley, typically occurring in late November, late January, early March and early April of each year. Allocation of water over a period of days results in a distinct irrigation peak for each event (Fig. 2a). Following each irrigation event, runoff flows through a network of natural and artificial drainage canals to coastal waters. Although the rate of drainage from the Yaqui Valley can be influenced by both watershed characteristics and management practice, runoff flows into the GOC within a few days of peak irrigation. In a few cases, when sufficient irrigation occurs in the days before the irrigation peak, runoff into the GOC precedes the peak; for the most part, however, irrigation waters arrive in the GOC on the day of peak irrigation or slightly after. For example, data from a conductivity–temperature–depth (CTD) recorder moored in the mouth of Bahía del Tóbari, an estuary located along the south coast of the Yaqui Valley, show a large drop in salinity and a smaller drop in temperature coincident with the peak irrigation date for January 2000 (E. Cruz-Colin, unpublished data).

To determine changes in phytoplankton biomass in the GOC driven by introduction of N in these pulses of runoff, chlorophyll *a* (Chl) data from the Sea-viewing Wide Field-of-view Sensor (SeaWiFS) were evaluated over a 5-year period. Arid conditions over the GOC allow generation of a remarkably complete time series of SeaWiFS data, with relatively few data gaps caused by cloud cover. Data extracted from a transect extending 100 km from Bahía del Tóbari across the GOC (Fig. 1), showed a strong annual cycle in phytoplankton biomass, typical of that seen throughout the GOC<sup>17</sup>. Chl concentrations were consistently highest in winter and spring, and lower in the summer months (Fig. 2b). These seasonal shifts were mirrored by changes in sea surface temperature (SST), measured using the Advanced Very High Resolution Radiometer (AVHRR); cooler SSTs in winter are associated with higher Chl levels, and vice versa (Fig. 2c).

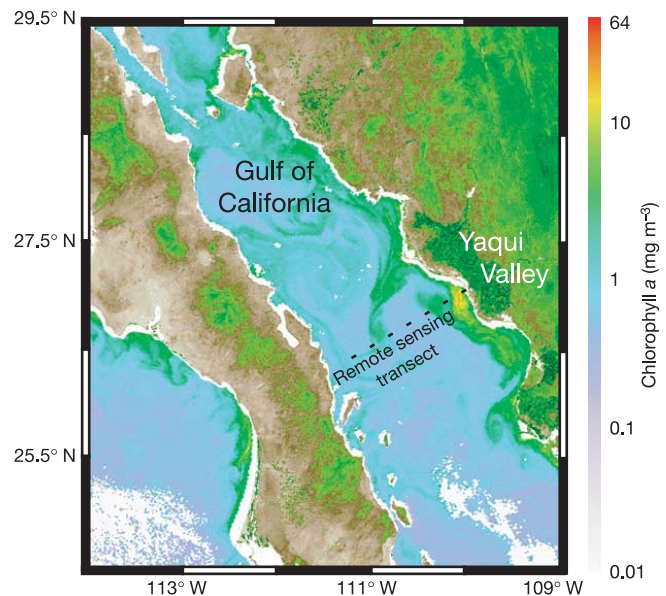


**Figure 1** SeaWiFS image of chlorophyll *a* in the GOC from 6 April 1998, one day after peak irrigation. Location of remote sensing transect is shown crossing an intense phytoplankton bloom. As indicated by the colour scale, Chl concentrations in the bloom are significantly higher than elsewhere in the GOC. On land, the productive agricultural fields of the Yaqui Valley are clearly visible in a MODIS-Aqua vegetation image (NDVI) from 4 April 2003, overlaid on ocean colour data.

Superimposed on this annual cycle were rapid increases in algal biomass—discrete phytoplankton blooms—clearly identifiable throughout the 5-year Chl record. These blooms were often intense, with Chl concentrations of  $>10 \text{ mg m}^{-3}$  (Figs 1 and 2b), and also quite extensive, reaching nearly 100 km across the GOC (Supplementary Video 1). Upwelling was a strong driver of many of these blooms, represented in the SST record by rapid drops in SST, as colder, nutrient-rich, deep waters were brought to the surface (Fig. 2c). Many other phytoplankton blooms, however, were associated with irrigation events in the Yaqui Valley (Fig. 2a, b). In fact, using Spearman's ranked correlation we find that periods of greater irrigation are significantly correlated with high Chl levels ( $r_s = 0.47$ ,  $P < 0.001$ ), despite hydrological and biogeochemical variability in the Yaqui Valley system that might mask this correlation. On the basis of this relationship, we suggest that up to 22% of the annual Chl variability in the GOC is related to N runoff from the Yaqui Valley.

Because remotely sensed SSTs are well correlated with nutrient concentrations over time, and inferred nutrient distributions are related to Chl concentrations<sup>18</sup>, a generalized linear model (GLM<sup>19</sup>) based on the relationship between SST and Chl was used to model natural Chl variability over time. Although the predictive ability of the model is limited by the strength of the SST–Chl relationship ( $r^2 = 0.45$ ,  $P < 0.01$ ), the model successfully removes seasonal Chl variability and winter and summer upwelling events (Fig. 2d), such as those observed in January 1998, January 1999 and August 2000. Residual Chl peaks (where Chl concentrations are greater than those predicted by the GLM) are persistent in autumn 1999 and in late spring and early summer 2001 and 2002. A similar decoupling between SST and Chl has been noted during summer in the GOC<sup>20</sup>, and was attributed to rapid heating of surface waters after upwelling, leaving a remnant Chl signal of upwelling but no SST signal.

In addition, there is a strong association between residual Chl

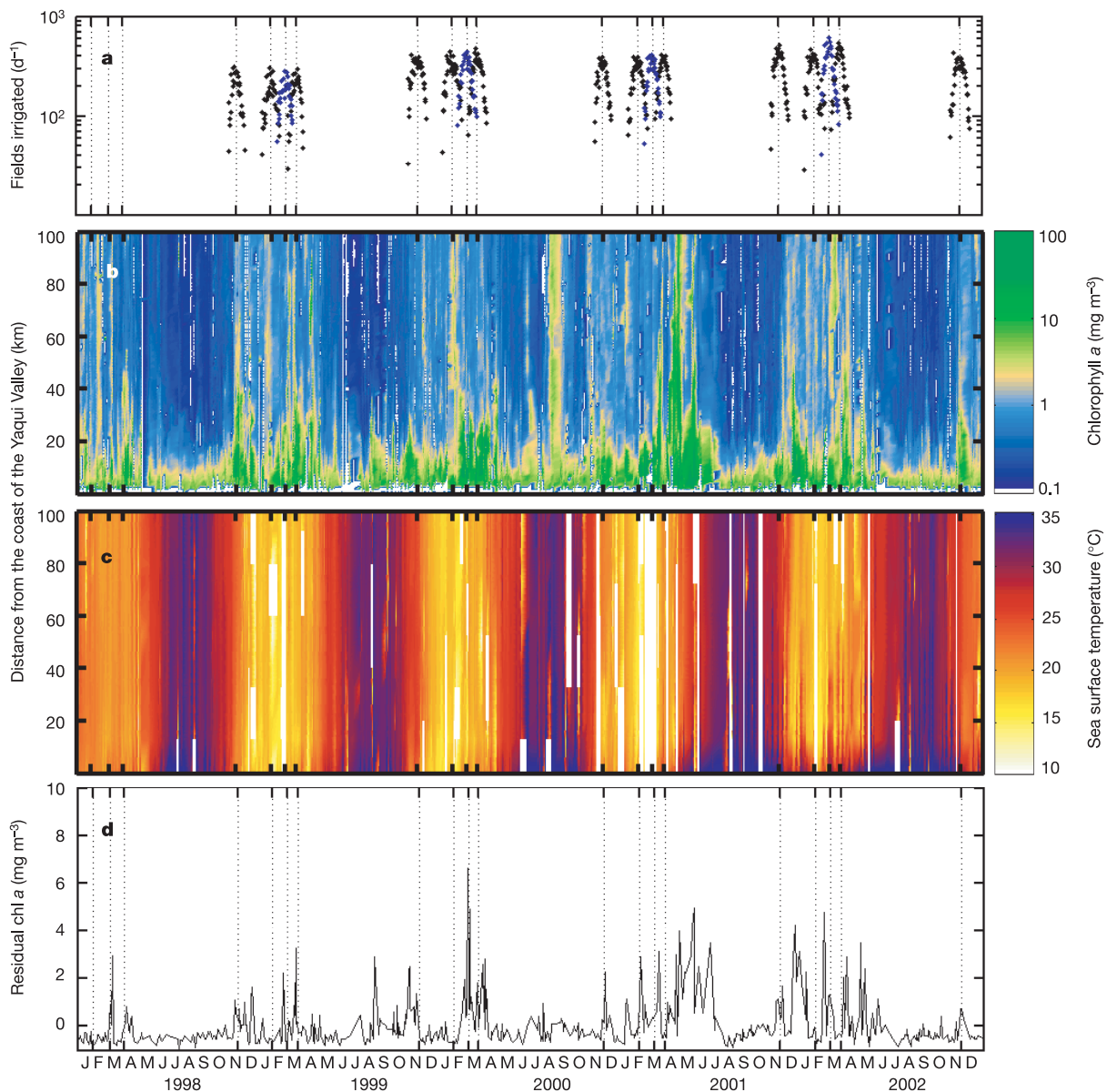


**Figure 2** Five-year time series. **a**, Irrigation allotment data. **b**, SeaWiFS chlorophyll *a* data. **c**, AVHRR SST data. **d**, Residual Chl values from best-fit GLM. Horizontal axis represents time from 1998–2002; calculated peak irrigation periods are denoted by

dotted lines and tick marks along the horizontal axis. Vertical axis in **b** and **c** represents distance across transect, colour bar on right shows corresponding Chl concentrations and SSTs.

Table 1 N-deficient marine regions and fertilizer use in adjacent developing agricultural regions

N-deficient marine region	Maximum N deficit (ref. no.)	Adjacent developing agricultural region	N fertilizer use ( $10^6$ megatonnes)		
			Value in 2000	Forecast 2020	Forecast 2050
Gulf of California Eastern tropical Pacific	16 $\mu\text{mol l}^{-1}$ (7) 12 $\mu\text{mol kg}^{-1}$ (4,5)	Tropical Americas	2.44	3.66	5.34
Benguela upwelling system	40 $\mu\text{mol kg}^{-1}$ (23)	Western Africa	0.246	0.469	0.711
Arabian Sea Bay of Bengal	12 $\mu\text{mol kg}^{-1}$ (24) 81 $\mu\text{mol l}^{-1}$ (25)	South Asia	14.4	21.9	33.9
South China Sea	1.2 $\mu\text{mol l}^{-1}$ (26)	Southeast Asia (Excluding China)	27.4 5.22	45.6 7.52	69.9 11.7
World total			80.9	129	187

peaks in winter and early spring and irrigation events in the Yaqui Valley (Fig. 2d). Of the 20 irrigation events in the Yaqui Valley from 1998–2002, peaks in both the unfiltered Chl record and the residual Chl record are directly associated with ten of them (Supplementary Fig. S1). Peaks lag the November 2000, April and November 2001, and April 2002 irrigation events by 3–5 days, bracket the March 1999 event (occurring 3–5 days before and after) and precede the November 1998 event by about 3 days. This correspondence between Yaqui Valley irrigation events and both unfiltered and residual Chl peaks strongly suggests that phytoplankton blooms in the GOC are stimulated by agricultural runoff from the Yaqui Valley. This association is particularly strong at the beginning and end of the crop cycle in November and April, when blooms consistently follow peak irrigation in the Yaqui Valley. It is less consistent in January (blooms in 2001 and 2002 were associated with runoff but those in 1998–2000 were not), perhaps because less N was lost from the valley during these irrigation events.

In general, the amount of N lost from the Yaqui Valley during irrigation events is sufficient to balance the N requirements of associated phytoplankton blooms. Associated blooms range in size from the 54 km<sup>2</sup> bloom in November 2002 to the 577 km<sup>2</sup> bloom in March 2000 (determined using SeaWiFS data), and estimates of annual N loss from the Yaqui Valley range from  $147 \times 10^6$  moles of N (based on a limited number of measurements in drainage canals<sup>13</sup>) to  $804 \times 10^6$  moles of N (based on N application rates of 250 kg N ha<sup>-1</sup> to  $2.25 \times 10^5$  ha of fields, with 20% N loss in surface waters<sup>16</sup>). If these losses are distributed equally over the four irrigation events every year,  $36.8 \times 10^6$  to  $201 \times 10^6$  moles of N are lost per irrigation event. Dividing these losses by a N deficit of 16  $\mu\text{M}$ , and assuming a mixed layer depth of 16–46 m (ref. 21), Yaqui Valley N losses during irrigation can support phytoplankton blooms in the GOC of 50–785 km<sup>2</sup>; this is in close agreement with bloom areas determined using SeaWiFS data. Although the supply of other nutrients such as P or iron (Fe) in runoff could potentially drive phytoplankton blooms in the GOC, particularly by increasing N-fixation rates<sup>22</sup>, we consider it unlikely. Phosphorus is found in excess throughout the GOC water column, with surface water concentrations >1  $\mu\text{M}$  (ref. 7), and Fe concentrations in Yaqui Valley drainage canals are low<sup>13</sup>. Because N losses occur in large pulses and in large part as ammonium<sup>13</sup>, we suspect that they effectively overwhelm the N-removal capacity of coastal systems<sup>2</sup>, flow into the strongly N-limited GOC and fuel the phytoplankton blooms observed in ocean colour imagery (Fig. 1 and Supplementary Video 1).

Large portions of the tropics and subtropics may be similarly vulnerable to N in agricultural runoff, as significant N depletion (via denitrification) occurs throughout the tropical and subtropical oceans, including the eastern tropical Pacific<sup>3–5</sup>, the Benguela upwelling system<sup>23</sup>, the Arabian Sea<sup>24</sup> and the Bay of Bengal<sup>25</sup> (Table 1). Nitrogen deficits are lower in the South China Sea, but

nutrient concentrations are low and N is strongly limiting during parts of the year<sup>26</sup>. These marine regions are located adjacent to rapidly developing agricultural areas in the tropical Americas, West Africa, South Asia, and Southeast Asia that will experience large increases in fertilizer use over the next few decades (Table 1). These increases outpace global trends (ref. 11, Table 1) and reflect a shift towards greater fertilizer consumption at low latitudes. In 2050, at least 27% of N fertilizer will be applied in regions adjacent to N-vulnerable marine ecosystems. Including China, this number more than doubles to 59% (Table 1). This represents a quantity greater than all N fertilizer currently applied worldwide.

Although only some portion of this applied N will reach the ocean, intensive agricultural systems like that in the Yaqui Valley are expected to develop in these regions over time<sup>27</sup>, and are likely to lead to similarly high N losses. In areas where runoff from these systems reaches N-vulnerable regions, as it does in the GOC, it represents a significant new source of N and strongly influences marine ecosystem processes. The downstream effects of runoff-driven phytoplankton blooms in the GOC are not yet known, but combined with fishing pressures<sup>28</sup>, carbon and energy become concentrated at lower trophic levels, with potentially significant effects for ecosystem structure and function. □

## Methods

### Irrigation data and timing

To determine peak irrigation dates, we fitted second-degree polynomials using least squares to irrigation allotment data from the Yaqui Valley Irrigation district. For these fits,  $r^2$  values were between 0.74 (January 2000) and 0.91 (April 2001). We calculated the peak irrigation date as the zero value of the first derivative of the polynomial. As data from early 1998 were not available, we instead used the best available estimate of peak irrigation from the Centro Internacional de Mejoramiento de Maíz y Trigo (CIMMYT, the International Wheat and Corn Improvement Center): days 31, 66 and 95 of 1998 (I. Ortiz-Monasterio, personal communication).

### Remote sensing data

Information regarding procurement and processing of SeaWiFS ocean colour data and AVHRR SST data can be found in the Supplementary Information.

### Generalized linear models

Time series data for use in the generalized linear model<sup>19</sup> were taken from imagery of the GOC off the coast of the Yaqui Valley. In order to capture the full spatial variability in bloom activity, we averaged values over a 30-km transect located 10 km off the coast of the Yaqui Valley. This transect is nearly perpendicular to the previous transect, allowing for coverage of all areas of input to the GOC from the southern half of the Yaqui Valley. We report the results of our 'best-fit' model, defined as that model which was most successful in reproducing Chl variability based on variability in SST, thereby minimizing residual Chl values. The best-fit model used a log-link function, and assumes the variables are gamma-distributed. The model takes the form  $\ln(\text{Chl}) = \beta_0 + \beta_1(\text{SST})$ , where  $\beta_0 = 3.41$  and  $\beta_1 = -0.0608$ . Model fitting was performed in glmab (MATLAB). Pearson residual values were calculated by subtracting modelled values from remotely sensed Chl data and scaling by the estimated standard deviation.

### Irrigation–bloom lead–lag analysis

To calculate the lead and lag times between irrigation peaks and Chl peaks, we fitted a series of smoothing splines to both unfiltered Chl data and residual Chl data. Smoothing

parameters of 0.25, 0.5 and 0.75 were used for each record, generating a total of 6 curve fits. We evaluated the first derivative of these fits at an interval of 3.125 days, the mean interval between satellite images. For each of the 6 derivatives, we defined two levels of sensitivity and identified peaks that exceeded these thresholds. For the 3 unfiltered Chl curves, sensitivities of 1 and 2 mg Chl m<sup>-3</sup> per 3.125-day interval were used; for the GLM residual Chl curves, sensitivities of 0.1 and 0.2 were used for all but the least smooth (parameter = 0.75) record, where sensitivities were 0.15 and 0.25. The zero value following each threshold-exceeding peak in the derivative was defined as a bloom event. Each of these 12 models identified between 20 and 92 bloom events, with significant overlap resulting in identification of 121 total bloom events (Supplementary Fig. S1). Identified blooms that occurred within a sampling interval of 3.125 days centred on irrigation peaks were considered to occur concurrently with irrigation; lead and lag timing was calculated relative to this. All statistical analyses were performed in MATLAB.

## Nitrogen deficit calculations

Nitrogen deficits were reported in the literature for the Eastern Tropical Pacific<sup>4,5</sup>, the Benguela upwelling system<sup>23</sup> and the Arabian Sea<sup>24</sup>. For the GOC, Bay of Bengal and South China Sea, deficits were calculated using the  $\Delta N$  formulation discussed previously<sup>23</sup> and based on data reported in the literature (GOC<sup>7</sup>, Bay of Bengal<sup>25</sup> and South China Sea<sup>26</sup>).

## Fertilizer data and projections

Data on use of N-based fertilizers was obtained from the United Nations Food and Agriculture Organization (FAO) Statistical Databases (<http://apps.fao.org>). World data includes all countries reporting to the FAO, and developing agricultural regions were defined as follows. Tropical Americas: Chile, Colombia, Costa Rica, Ecuador, El Salvador, Guatemala, Mexico, Nicaragua, Panama and Peru; Western Africa: Angola, Benin, Burkina Faso, Cameroon, Cape Verde, Côte d'Ivoire, Democratic Republic of Congo, Gabon, Gambia, Ghana, Guinea, Guinea-Bissau, Liberia, Mali, Mauritania, Namibia, Niger, Nigeria, Republic of Congo, Senegal, Sierra Leone and Togo; South Asia: Bangladesh, Bhutan, India, Nepal, Pakistan and Sri Lanka; Southeast Asia: Brunei Darussalam, Cambodia, China, Indonesia, Laos, Malaysia, Myanmar, Philippines, Singapore, Thailand and Vietnam. Using a previously described approach<sup>11</sup>, we found strong linear increases in fertilizer use over time in all regions, with  $r^2$  values between 0.90 (Western Africa) and 0.97 (Southeast Asia). We projected these relationships forward to 2020 and 2050 to calculate fertilizer use.

Received 1 November 2004; accepted 17 January 2005; doi:10.1038/nature03370.

1. Tyrrell, T. The relative influences of nitrogen and phosphorus on oceanic primary production. *Nature* **400**, 525–531 (1999).
2. Corredor, J. E., Howarth, R. W., Twilley, R. R. & Morell, J. M. Nitrogen cycling and anthropogenic impact in the tropical interamerican seas. *Biogeochemistry* **46**, 163–178 (1999).
3. Gruber, N. & Sarmiento, J. L. Global patterns of marine nitrogen fixation and denitrification. *Glob. Biogeochem. Cycles* **11**, 235–266 (1997).
4. Deutsch, C., Gruber, N., Key, R. M., Sarmiento, J. L. & Ganachaud, A. Denitrification and N<sub>2</sub> fixation in the Pacific Ocean. *Glob. Biogeochem. Cycles* **15**, 483–506 (2001).
5. Tyrrell, T. & Law, C. S. Low nitrate-phosphate ocean ratios corrected. *Nature* **393**, 318 (1998).
6. Zeitzschel, B. Primary productivity in the Gulf of California. *Mar. Biol.* **3**, 201–207 (1969).
7. Alvarez-Borrego, S., Rivera, J. A., Gaxiola-Castro, G., Acosta-Ruiz, M. & Schwartzlose, R. A. Nutrientes en el Golfo de California. *Ciencias Marinas* **5**, 53–71 (1978).
8. Alvarez-Borrego, S. in *A New Island Biogeography of the Sea of Cortes* (eds Case, T. J., Cody, M. L. & Ezcurra, E.) 41–59 (Oxford Univ. Press, New York, 2002).
9. Beron-Vera, F. J. & Ripa, P. Three-dimensional aspects of the seasonal heat balance in the Gulf of California. *J. Geophys. Res.* **105**, 11441–11457 (2000).
10. Galloway, J. N. *et al.* The nitrogen cascade. *Bioscience* **53**, 341–356 (2003).
11. Tilman, D. G. *et al.* Forecasting agriculturally driven global environmental change. *Science* **292**, 281–284 (2001).
12. Naylor, R., Falcon, W. P. & Puente-Gonzalez, A. *Policy Reforms and Mexican Agriculture: Views from the Yaqui Valley* (CIMMYT Economics Program Paper no. 01–01, CIMMYT, Mexico City, 2001).
13. Harrison, J. A. *Nitrogen Dynamics and Greenhouse Gas Production in Yaqui Valley Surface Drainage Waters*. PhD thesis, Stanford Univ (2003).
14. Harrison, J. A. & Matson, P. A. Patterns and controls of nitrous oxide emissions from waters draining a subtropical agricultural valley. *Glob. Biogeochem. Cycles* **17**, 1080, doi:10.1029/2002GB001991 (2003).
15. Matson, P. A., Naylor, R. & Ortiz-Monasterio, I. Integration of environmental, agronomic, and economic aspects of fertilizer management. *Science* **280**, 112–115 (1998).
16. Riley, W. J., Ortiz-Monasterio, I. & Matson, P. A. Nitrogen leaching and soil nitrate, nitrite, and ammonium levels under irrigated wheat in Northern Mexico. *Nutrient Cycling Agroecosyst.* **61**, 223–236 (2001).
17. Kahr, M., Marinone, S. G., Lluch-Cota, S. E., Pares-Sierra, A. & Mitchell, B. G. Ocean color variability in the Gulf of California: scales from days to ENSO. *Deep-Sea Res. II* **51**, 139–146 (2004).
18. Switzer, A. C., Kamykowski, D. & Zentara, S.-J. Mapping nitrate in the global ocean using remotely sensed sea surface temperature. *J. Geophys. Res.* **108**, 3280 (2003).
19. McCullagh, P. & Nelder, J. A. *Generalized Linear Models* (Chapman and Hall, London, 1989).
20. Pegau, W. S., Boss, E. & Martinez, A. Ocean color observations of eddies during the summer in the Gulf of California. *Geophys. Res. Lett.* **29**, doi:10.1029/2001GL014076 (2002).
21. Gaxiola-Castro, G., Alvarez-Borrego, S., Lavin, M., Zirino, A. & Najera-Martinez, S. Spatial variability of the photosynthetic parameters and biomass of the Gulf of California phytoplankton. *J. Plankton Res.* **21**, 231–245 (1999).
22. Mills, M. M., Ridame, C., Davey, M., La Roche, J. & Gelder, R. J. Iron and phosphorus co-limit nitrogen fixation in the eastern tropical North Atlantic. *Nature* **429**, 292–294 (2004).
23. Tyrrell, T. & Lucas, M. I. Geochemical evidence of denitrification in the Benguela upwelling system. *Continental Shelf Res.* **22**, 2497–2511 (2002).

24. Howell, E. A., Doney, S. C., Fine, R. A. & Olson, D. B. Geochemical estimates of denitrification in the Arabian Sea and the Bay of Bengal during WOCE. *Geophys. Res. Lett.* **24**, 2549–2552 (1997).
25. Valsaraj, C. P. & Rao, V. N. R. Nitrogen limitation in the tropical waters of the Bay of Bengal. *Hydrobiologia* **286**, 139–148 (1994).
26. Chen, Y. L., Chen, H.-Y., Karl, D. M. & Takahashi, M. Nitrogen modulates phytoplankton growth in spring in the South China Sea. *Continental Shelf Res.* **24**, 527–541 (2004).
27. Tilman, D. G., Cassman, K. G., Matson, P. A., Naylor, R. & Polasky, S. Agricultural sustainability and intensive production practices. *Nature* **418**, 671–677 (2002).
28. Sala, E., Aburto-Oropeza, O., Reza, M., Paredes, G. & Lopez-Lemus, L. G. Fishing down coastal food webs in the Gulf of California. *Fisheries* **29**, 19–25 (2004).

Supplementary Information accompanies the paper on [www.nature.com/nature](http://www.nature.com/nature).

**Acknowledgements** We are grateful for funding from the David and Lucile Packard Foundation and the US NSF Graduate Research Fellowship Program. Thanks to G. van Dijken and R. Labiosa for remote sensing support, I. Ortiz-Monasterio for irrigation data, E. Cruz-Colin for sharing unpublished data, and K. Beman for editorial advice. We thank P. Vitousek and R. Dunbar for comments on an earlier draft of this manuscript.

**Competing interests statement** The authors declare that they have no competing financial interests.

**Correspondence** and requests for materials should be addressed to J.M.B. ([beman@stanford.edu](mailto:beman@stanford.edu)).

## The global distribution of clinical episodes of *Plasmodium falciparum* malaria

Robert W. Snow<sup>1,2</sup>, Carlos A. Guerra<sup>3</sup>, Abdisalan M. Noor<sup>1</sup>, Hla Y. Myint<sup>4</sup> & Simon I. Hay<sup>1,3</sup>

<sup>1</sup>Public Health Group, KEMRI/Wellcome Trust Research Laboratories PO Box 43640, 00100 Nairobi, Kenya

<sup>2</sup>Centre for Tropical Medicine, John Radcliffe Hospital, University of Oxford, Oxford OX3 9DS, UK

<sup>3</sup>TALA Research Group, Tinbergen Building, Department of Zoology, University of Oxford, South Parks Road, Oxford OX1 3PS, UK

<sup>4</sup>Faculty of Tropical Medicine, Mahidol University, Bangkok 10400, Thailand

Interest in mapping the global distribution of malaria is motivated by a need to define populations at risk for appropriate resource allocation<sup>1,2</sup> and to provide a robust framework for evaluating its global economic impact<sup>3,4</sup>. Comparison of older<sup>5–7</sup> and more recent<sup>1,4</sup> malaria maps shows how the disease has been geographically restricted, but it remains entrenched in poor areas of the world with climates suitable for transmission. Here we provide an empirical approach to estimating the number of clinical events caused by *Plasmodium falciparum* worldwide, by using a combination of epidemiological, geographical and demographic data. We estimate that there were 515 (range 300–660) million episodes of clinical *P. falciparum* malaria in 2002. These global estimates are up to 50% higher than those reported by the World Health Organization (WHO) and 200% higher for areas outside Africa, reflecting the WHO's reliance upon passive national reporting for these countries. Without an informed understanding of the cartography of malaria risk, the global extent of clinical disease caused by *P. falciparum* will continue to be underestimated.

The Global Burden of Diseases programme of the WHO has attempted to enumerate the health consequences of malaria infection<sup>8,9</sup>. Because the African region has a notoriously weak system of reporting infectious diseases, epidemiological evidence from carefully conducted prospective, 'active' case-detection studies of malaria morbidity, disability and mortality in populations living